Modeling techniques for BBU modes in induction linac cavities

Stanley Humphries, Ph.D.

E mail: techinfo@fieldp.com
Internet: https://www.fieldp.com

1 Introduction

The beam breakup (BBU) instability may affect beam quality in high-current linear induction accelerators. Briefly, a transverse displacement of the beam can transfer energy to resonant modes in the acceleration cavities of the type TM_{1n0}. These modes have an axial electric field (E_z) at the beam position that reverses direction crossing the axis. For the discussion, assume that the electric field reverses in the y direction. In this case, TM_{0n0} modes have a concentration of transverse magnetic field (B_x) at the beam position. The fields cause beam deflections in y that can drive the mode at increased amplitude in subsequent cavities. The result is the growth of beam displacement moving downstream with increasing resonant mode amplitude. There have been several theoretical and experimental studies of BBU electromagnetic modes in the DARHT 1 and DARHT 2 accelerators. My task was to set up models using the **Aether** three-dimensional electromagnetic code to enable comparisons of mode properties between different cavity configurations of the DARHT 1 and DARHT 2 accelerators as well as future induction accelerator projects. **Aether** is optimized for personal computers, making it a convenient study tool for DARHT personnel.

Initially, I concentrated on the DARHT Mod2 geometry of Fig. 1. Electromagnetic calculations can generate a wealth of information, so it is important to know exactly what to look for. My strategy was to start from a known point (the TM_{110} mode in a metal cylindrical cavity) and to make incremental changes to arrive at the structure of Fig. 1. In the process, I found some useful physical insights that I will summarize in this report.[1]

2 Transverse mode in a cylindrical metal cavity

It is useful to start with mode calculations in a simple geometry for two reasons:

- We can compare numerical results to analytic predictions.
- It is easier to display and to understand field variations compared to those in the convoluted geometry of the DARHT cavity.

Accordingly, I will discuss **Aether** calculations for modes of the type TM_{1n0} in a cylindrical cavity. I used dimensions comparable to those of the DARHT cavities: radius $R = 23.5$ cm and length $D = 3.0$ cm. Although the cavity has two-dimensional symmetry, it is necessary to use a three-dimensional code to find modes of type $m = 1$. The first step is the creation of an appropriate mesh using the **MetaMesh** program[2] An element size of 0.50 cm gives good accuracy and short run time. I set a constraint that modes of interest must have $E_z = 0.0$ along the line $y = 0.0$. In other words, the $m = 1$ modes satisfy the symmetry condition

$$E_z(x, y, z) = -E_z(x, -y, z). \tag{1}$$

[1]The calculations in this report deal with cold-cavity modes where ferrites are assumed to be isotropic with uniform properties. The characteristics of ferrite in an induction linac are much more complex under load where saturation effects are important.

[2]For brevity, I will not list contents of input files in this report. The archive `BBU01.zip` contains the complete set of input files to generate the results of this report arranged by section.

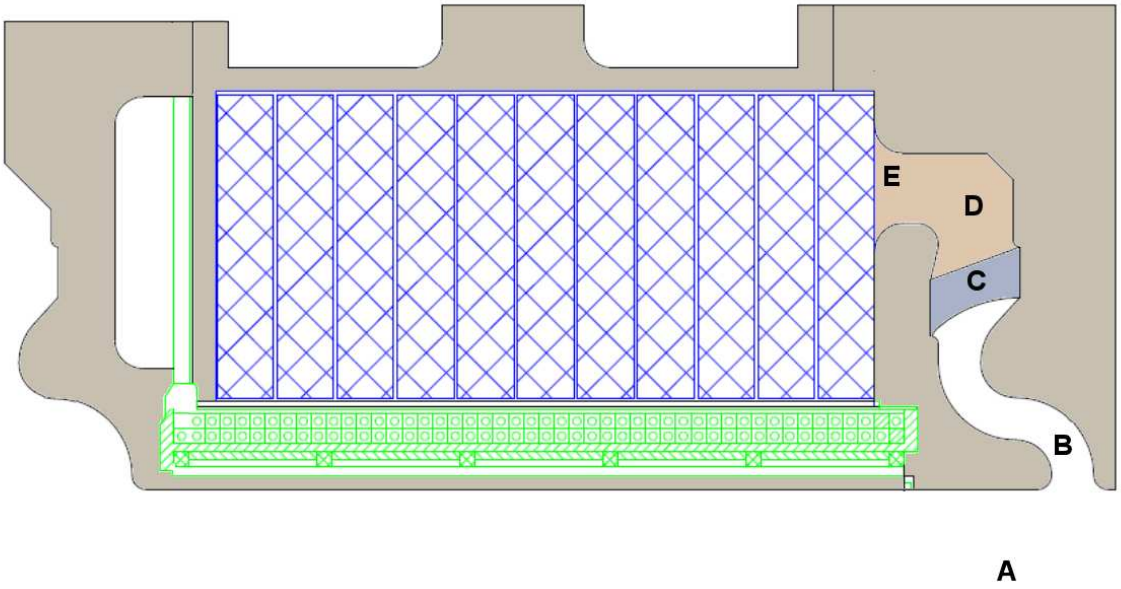

Figure 1: DARHT Mod2 acceleration cavity, a figure of revolution about the axis at the bottom. *A*) Beam tube of radius 7.41 cm. *B*) Vacuum region. *C*) Rexolite insulator. *D*) Transformer oil. *E*) Surface of the ferrite stack.

Equation 1 implies that it is not necessary to model the full cavity. Instead, we can model the region $y \geq 0.0$ with a metal boundary condition at $y = 0.0$. This approach has two advantages:

- Halving the number of elements reduces the run time.
- Modes of type $m = 0$ are suppressed.

The second condition helps to reduce distractions when we address more complex cavity geometries.

The technique in **MetaMesh** is to fill the solution volume (a box with sides $L_x = 48.0$ cm, $L_y = 24.5$ cm and $L_z = 4.0$ cm) with elements that have the property of metal. Then, we carve a cylindrical volume of radius 23.5 cm and length 3.0 cm and put a sheet of thickness $L_y = 0.5$ cm at $y = -0.25$ cm to define the symmetry boundary. The final region (a cube with sides 1.0 cm) is placed near the point of maximum expected electric field. This region is set as a current source (j_z) to excite the electromagnetic mode. Figure 2 shows the resulting mesh. Note that the mesh is regular rather than conformal. The time-domain, finite-element formulation of **Aether** is based on box elements. Therefore, the **MetaMesh** input script has no `SURFACE` fitting commands and includes the command `SMOOTH 0`.

Resonant-mode calculations with **Aether** involve two operations:

- Identification of resonant frequencies by excitation of the cavity with a broad spectrum pulse followed by Fourier analysis of probe signals.

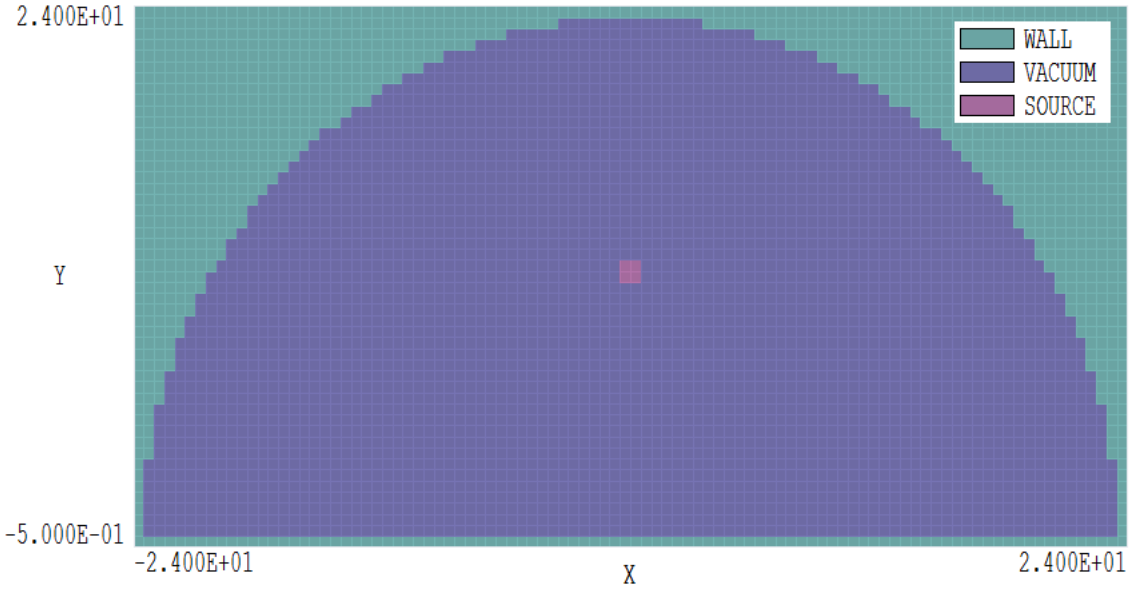

Figure 2: Mesh to calculate the TM_{110} mode of a cylindrical cavity, cross-section at $z = 0.0$ cm.

- A field calculation at the identified frequency.

I made resonance and field calculations for both the half and full geometries. The motivations where 1) to validate use of the symmetry condition and 2) to generate illustrations showing the full mode. A probe recorded H_x near the axis. The predicted frequency was

$$f_{110} = \frac{3.832c}{2\pi R} = 778.6 \quad \text{MHz}. \tag{2}$$

The run times for resonance search were 24 seconds for the half cavity and 78 seconds for the full geometry. Figure 3 shows the Fourier analysis of the probe signal. Note that the resonance peak had a non-width, the result of discretization in space and time. Using a peak peak-detection algorithm, **Aether** yielded the following resonant frequencies: 779.32 MHz for the full cavity and 779.37 MHz for the half cavity.

I made field calculations for both configurations at the resonant frequencies. In this case, the solution times were 4 seconds for the half solution and 14 seconds for the full solution. Figure 4 shows the distribution of E_z and H_x at peak amplitude in a plane normal to z. The areas of high electric field represent axial displacement current between the cavity walls. The return current flows either through the walls around the outer boundary or across the axis to feed the displacement current in the other half-plane in y. As a result, there are regions of strong H_x with opposite polarity near the axis and outer wall. Figure 5 (taken from my book **Charged Particle Beams**) clarifies the nature of the mode through an equivalent circuit.

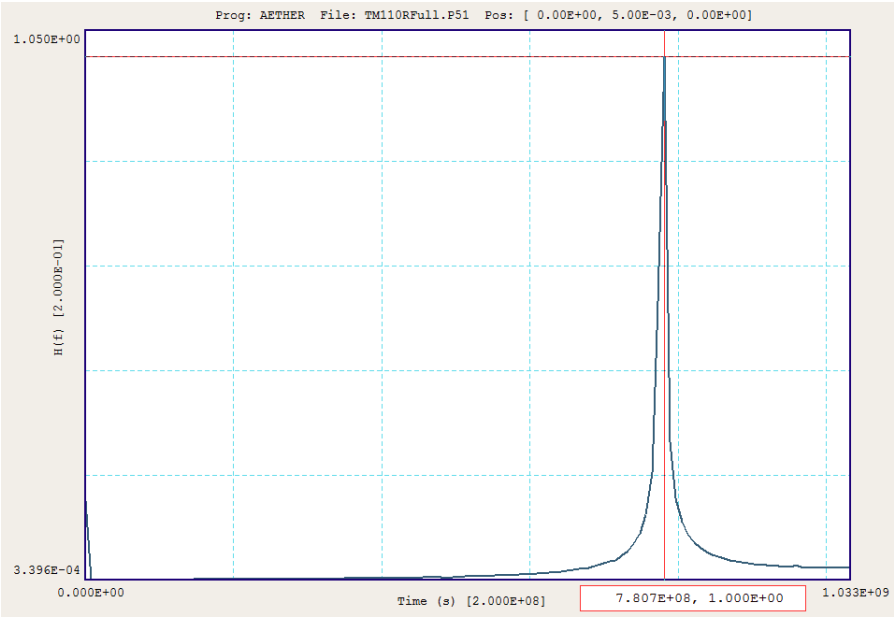

Figure 3: Fourier analysis of H_x near the axis of a cylindrical cavity with $R = 23.5$ cm. The excitation pulse covered the range from 300 MHz to 1300 MHz.

In review, the half-cavity setup had three features to ensure a unambiguous identification of the desired mode:

- The metal boundary condition at $y = 0.0$ favored modes of type $m = 1$.
- The excitation source of j_z was placed near the point of maximum expected electric field E_z.
- The probe to detect H_x was placed near the point of maximum expected magnetic field.

The same methods could be used to create higher-order modes of type TM_{1n0}, with predicted frequencies $f_{120} = 7.016c/2\pi R = 1425$ MHz and $f_{130} = 10.175c/2\pi R = 2067$ MHz. These modes are not be of interest for DAHRT cavity calculations because of the possibility of radiation transport along the large beam pipe (Fig. 1). The cutoff frequencies for modes in the pipe of radius 0.0741 m are 1550 MHz for TM modes and 1180 MHz for TE modes. Because energy can move freely along the beam pipe above the cutoff, high-frequency cavity resonances will not occur. In the remainder of this report, I will consider only the fundamental BBU mode.

Given an understanding of the TM_{110} mode, we can identify the computational challenges presented by the DARHT cavity by noting the differences between the simple cylindrical cavity and the system of Fig. 1. The DARHT geometry is clearly more complex, but this issue is handled easily by a finite-element code – the DARHT cavity can be viewed as a twisted cylinder. Other differences are more significant:

- Outer regions have a dielectric fill ($\epsilon_r > 1.0$).

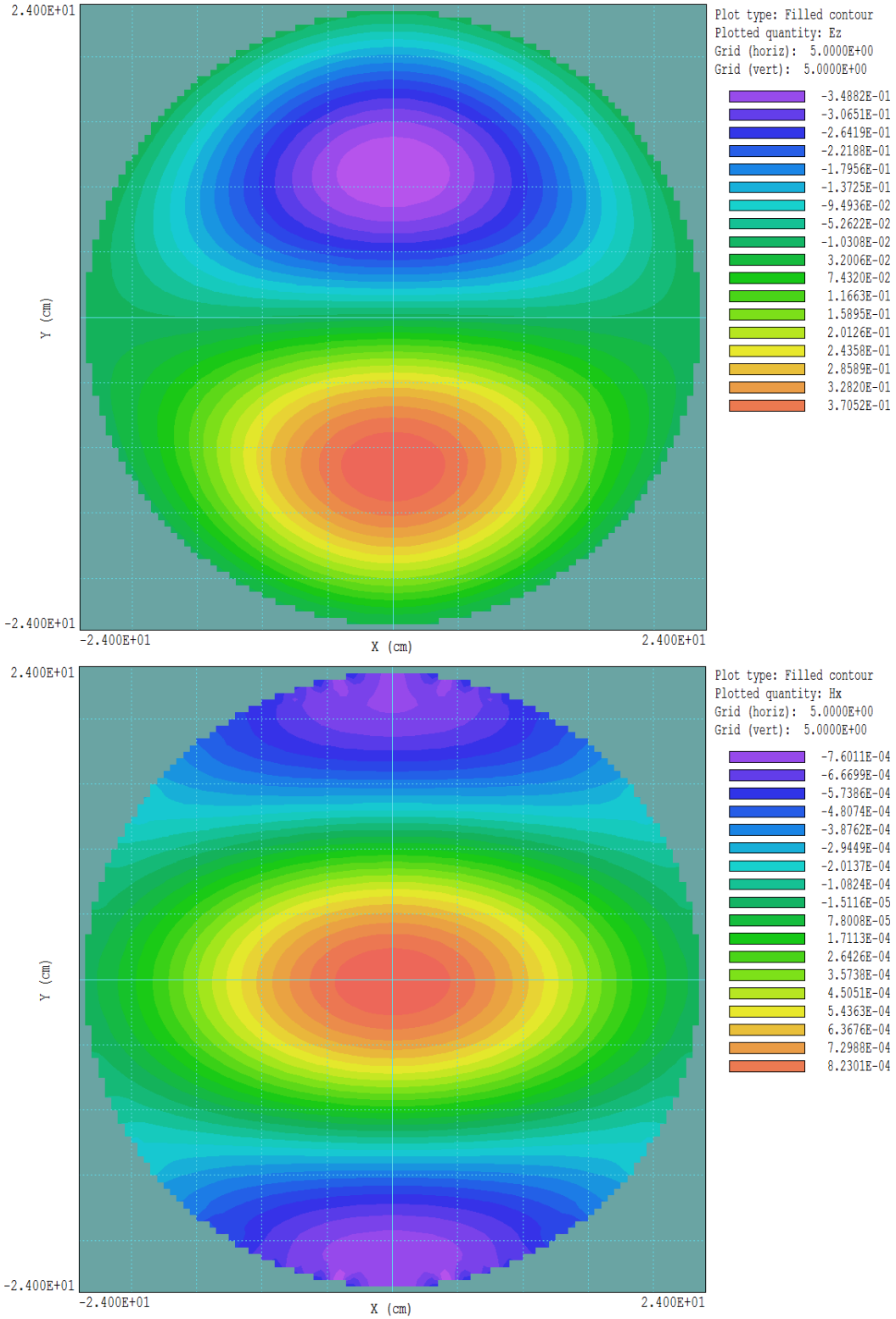

Figure 4: Full cavity calculation of the TM_{110} mode in a cylindrical cavity. Plots of E_z (at 0.0° phase) and H_x (at 90.0° phase) in the plane $z = 0.0$ cm.

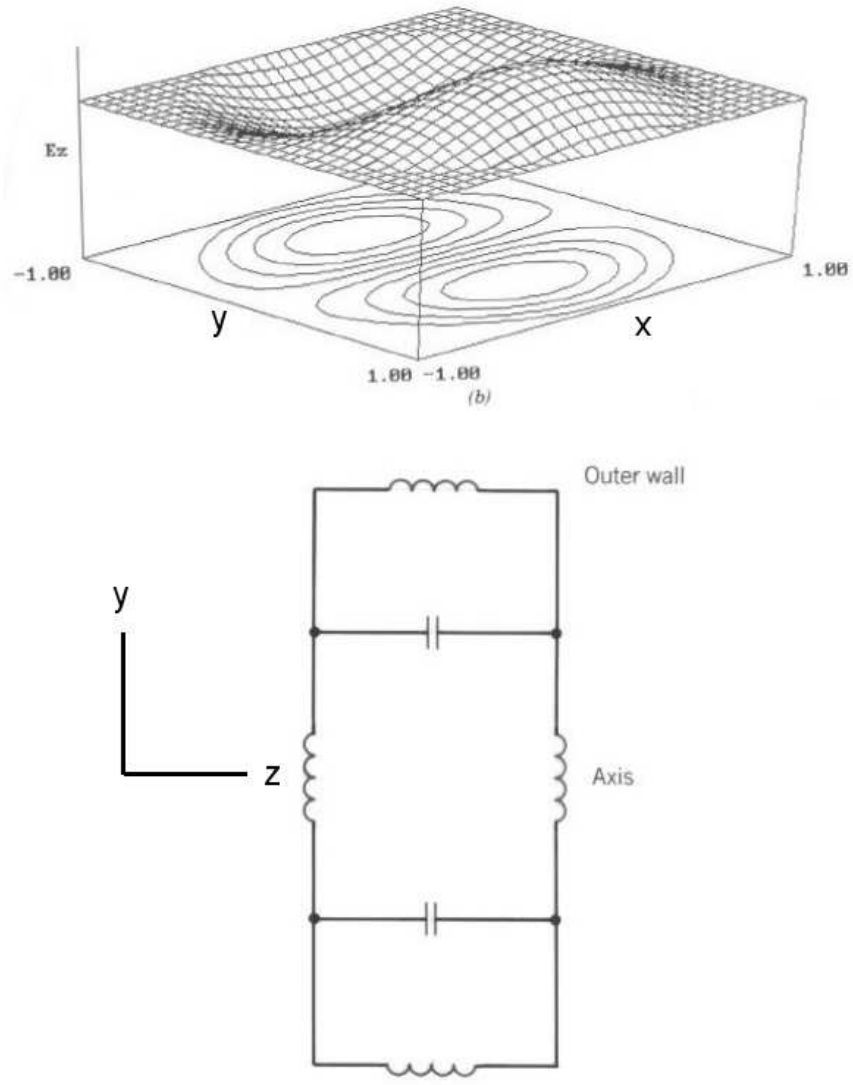

Figure 5: Characteristics of the TM_{110} mode. a) Electric field distribution. b) Equivalent circuit model.

- The large-diameter beam pipe shifts the resonant frequency and perturbs the field distribution near the axis.
- The outer boundary is a ferrite rather than a metal wall.

The remainder of this section addresses the effect of dielectrics on the TM_{110} mode of a cylindrical cavity. Section 3 discusses the effects of the beam pipe while Sect. 4 reviews methods to represent a ferrite boundary in a finite-element calculation.

It is easy to modify the cylindrical-cavity solution to include dielectric regions. I assigned a relative dielectric constant $\epsilon_r = 2.3$ to the region $15.0 \leq r \leq 23.5$ cm. The choice ϵ_r was approximately the average of values for transformer oil and the Rexolite insulator of the DARHT cavity. The value 15.0 cm was close to that of the inner radius of the DARHT insulator. The top illustration in Fig. 6a shows the mesh in a plane normal to z. The effect of the dielectric region was to increase the capacitance in Fig. 5*b*, lowering the resonant frequency from 779.3 MHz to 637.1 MHz. There was a small change in the field morphology, as shown in Fig. 6. The middle illustration shows contours $|H_x|$ for the bare cavity, while the distribution in the lower illustration includeds the effect of the dielectric. Because of the increased capacitance at large radius, a higher fraction of return current flowed through the outer wall.

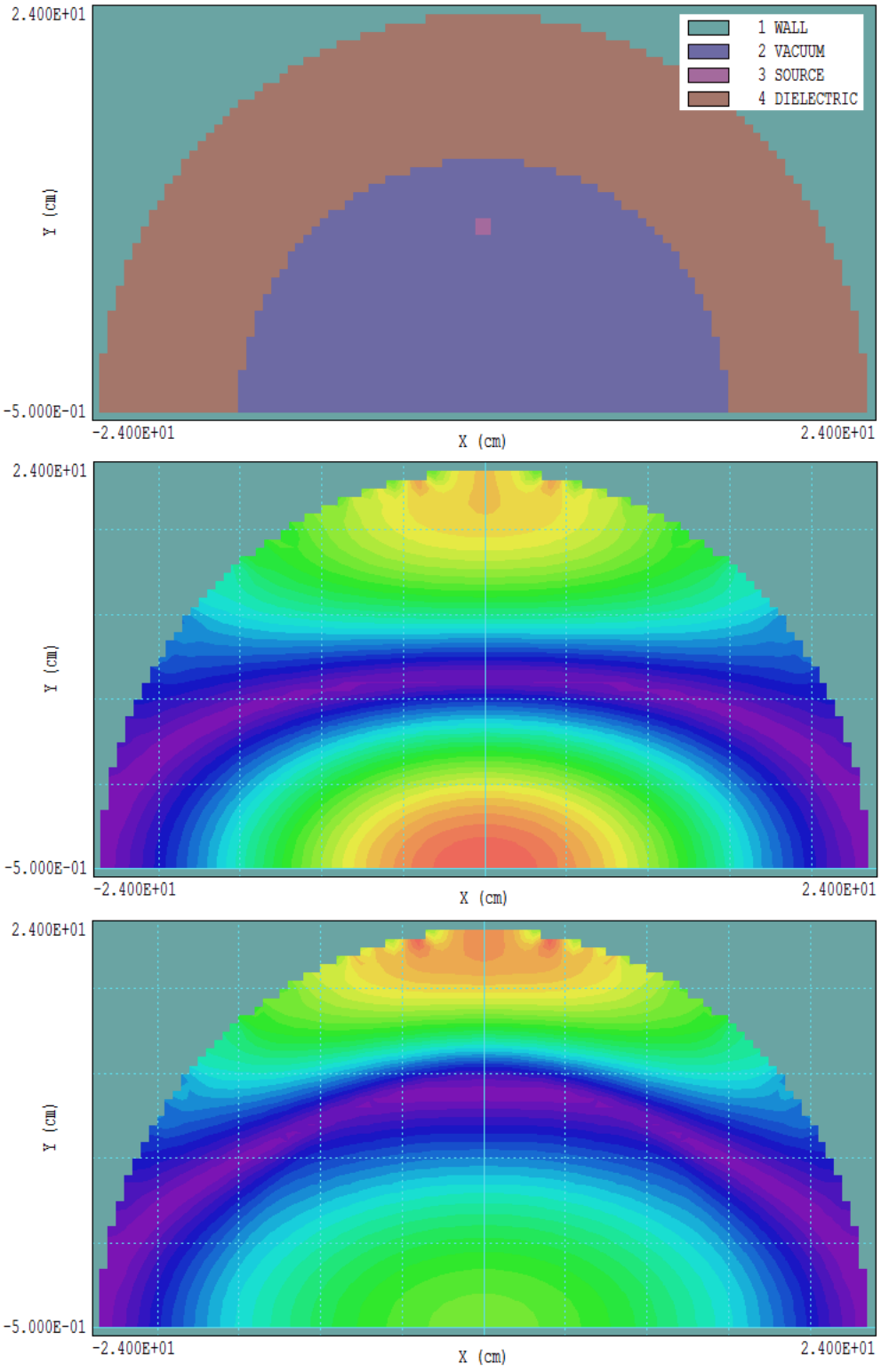

Figure 6: Effect of a dielectric outer region on the TM_{110} mode. Top: mesh in a plane normal to z. Center: distribution of $|H_x|$ with the dielectric relative permeability set to $\epsilon_r = 1.0$. Bottom: distribution of $|H_x|$ with the dielectric relative permeability set to $\epsilon_r = 2.3$.

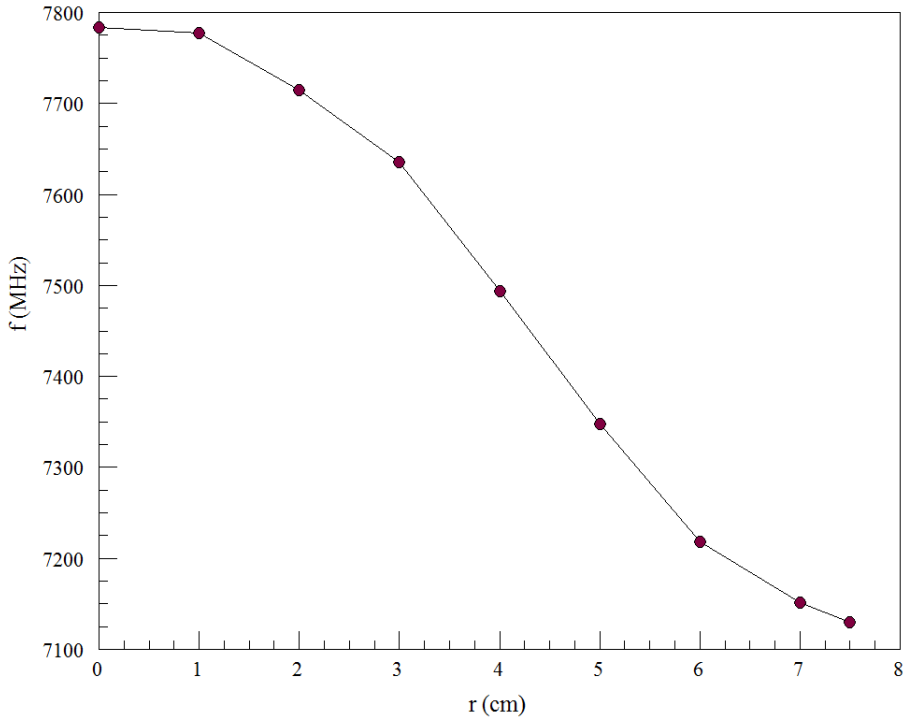

Figure 7: Variation of f_{110} as a function of beam pipe radius. Cylindrical cavity with $R = 23.5$ cm and $D = 2.0$ cm.

3 Effect of the beam pipe

The presence of an axi-centered beam pipe perturbs the flow of current of the TM_{110} mode between the upper and lower halves of the cavity. Current must follow a longer path, raising the effective inductance across the axis (Fig. 5) and modifying the field distribution near the axis. Therefore, we expect a decrease in the resonant frequency with increasing beam pipe radius. I created a set of calculations based on a bare cylindrical cavity with $R = 23.5$ cm and $D = 2.0$ cm (close to minimum gap width of DAHRT cavity). I added beam pipes of different sizes up to a maximum radius of 7.5 cm. On issue is how to set boundary conditions where the pipe intersects the axial boundaries of the solution volume. The lowest-frequency transverse mode is evanescent in even the largest pipe, so the field levels should drop off quickly moving upstream and downstream. Accordingly, I constructed solutions with beam pipes of depth 14.0 cm terminated with a metal boundary.

I set up a series of eight mesh-definition files for beam pipe radii from 0.0 cm to 7.5 cm. I also made resonance calculations for each geometry and field calculations for radii of 0.0 cm and 7.5 cm . Figure 7 shows the frequency of the TM_{110} mode as a function of the beam pipe radius. A pipe of radius 7.5 cm lowers the frequency by a factor 0.916. More significant for the BBU instability, the flow of return current around the pipe aperture strongly influences the field distribution near the axis. For example, Fig. 8 shows the variation of $|H_x|$ in the plane $z = 0.0$ for beam pipe radii of 0.0 cm and 7.5 cm. The solutions have been normalized to the same total field energy. A standard assumption in BBU calculations that the deflection magnetic field is approximately uniform over the beam cross section clearly does not hold.

In addition to the strong spatial variation, introduction of the beam pipe also reduces the value of H_x integrated over z. There is also a change in E_z, as shown in Fig. 9. The beam pipe introduces a non-linear variation, so the assumption of approximately uniform gradient dE_z/dy over the beam volume is invalid.

Finally, Fig. 10 shows plots of field variations in the plane $x = 0.0$ cm. Slice plots in this plane will be useful when we discuss the irregular geometry of the DARHT cavity. It is important to understand the type of field variations to expect for transverse modes. The top sections show variations $|H_x|$ and the bottom section show $|E_z|$. For each quantity, the upper illustration corresponds to the ideal TM_{110} mode in a cylindrical cavity with no beam pipe. Consistent with Fig. 4, the deflecting magnetic field exhibits a maximum at the axis and the outer radius. It passes through zero in the region of high electric field. In contrast, with the beam pipe included the zero crossing shifts inward and the field value is low near the axis. Furthermore, H_x near the axis extends upstream and downstream over a larger region than the cavity width. The lower sections show the non-linear variation of E_z near the axis.

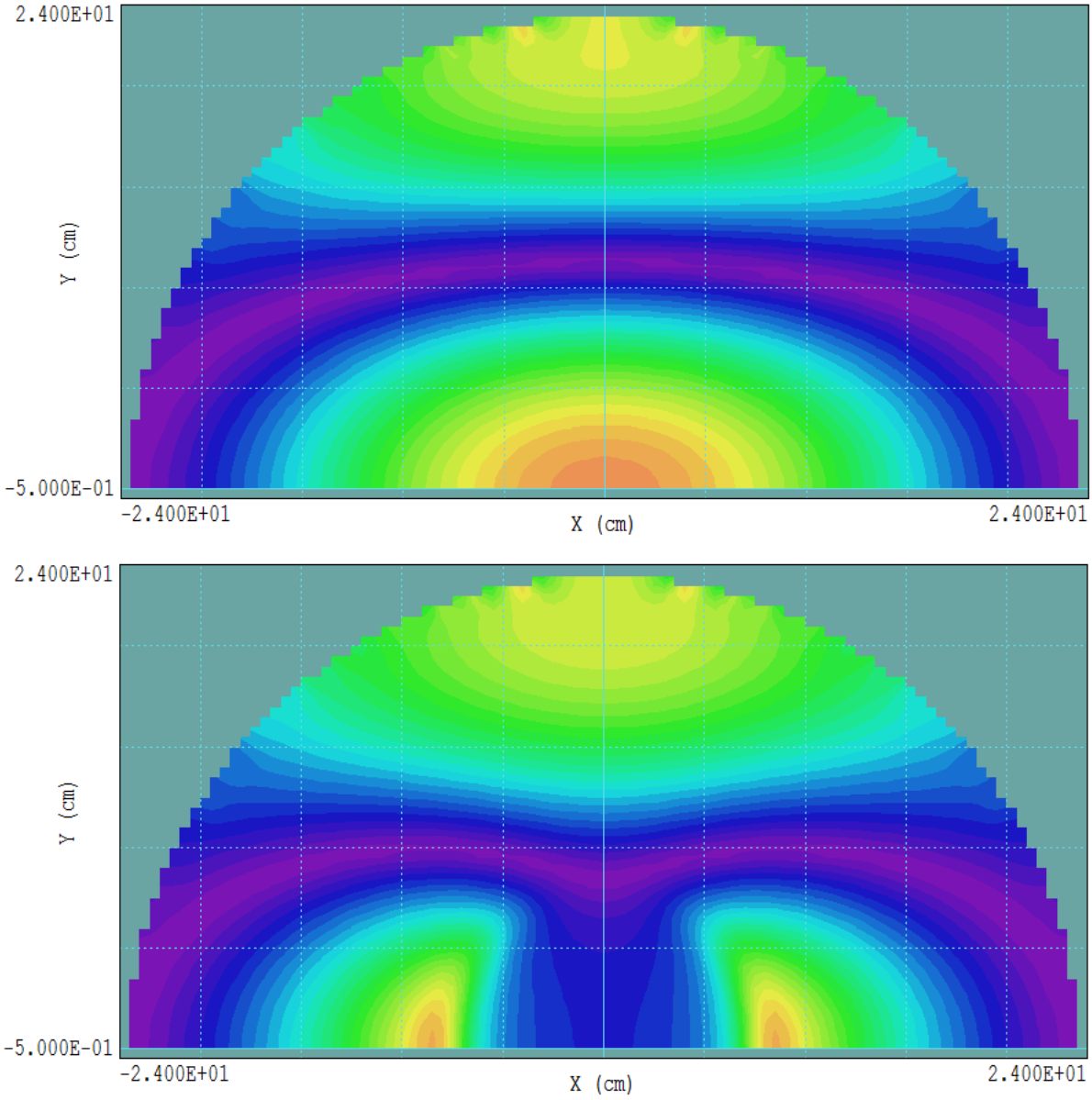

Figure 8: Distribution of $|H_x|$ for the TM_{110} mode in the plane $z = 0.0$ cm. Top: No beam pipe. Bottom: Beam pipe of radius 7.5 cm.

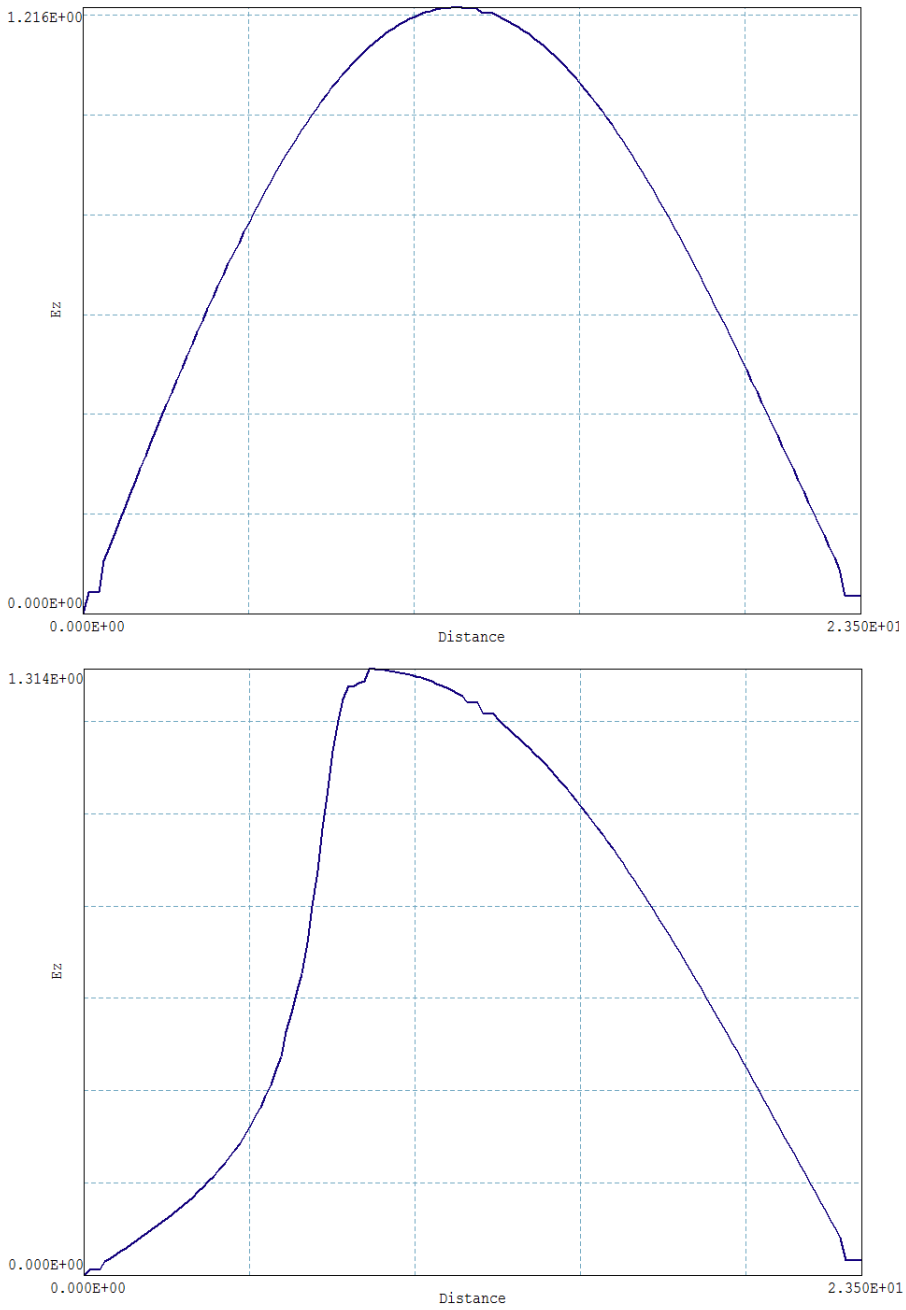

Figure 9: Variation of $|E_z|$ along y for the TM_{110} mode at $x = 0.0$ cm, $z = 0.0$. Top: cylindrical cavity, $R = 23.5$ cm, $D = 2.0$ cm. Bottom: cavity with beam pipe of radius 7.5 cm.

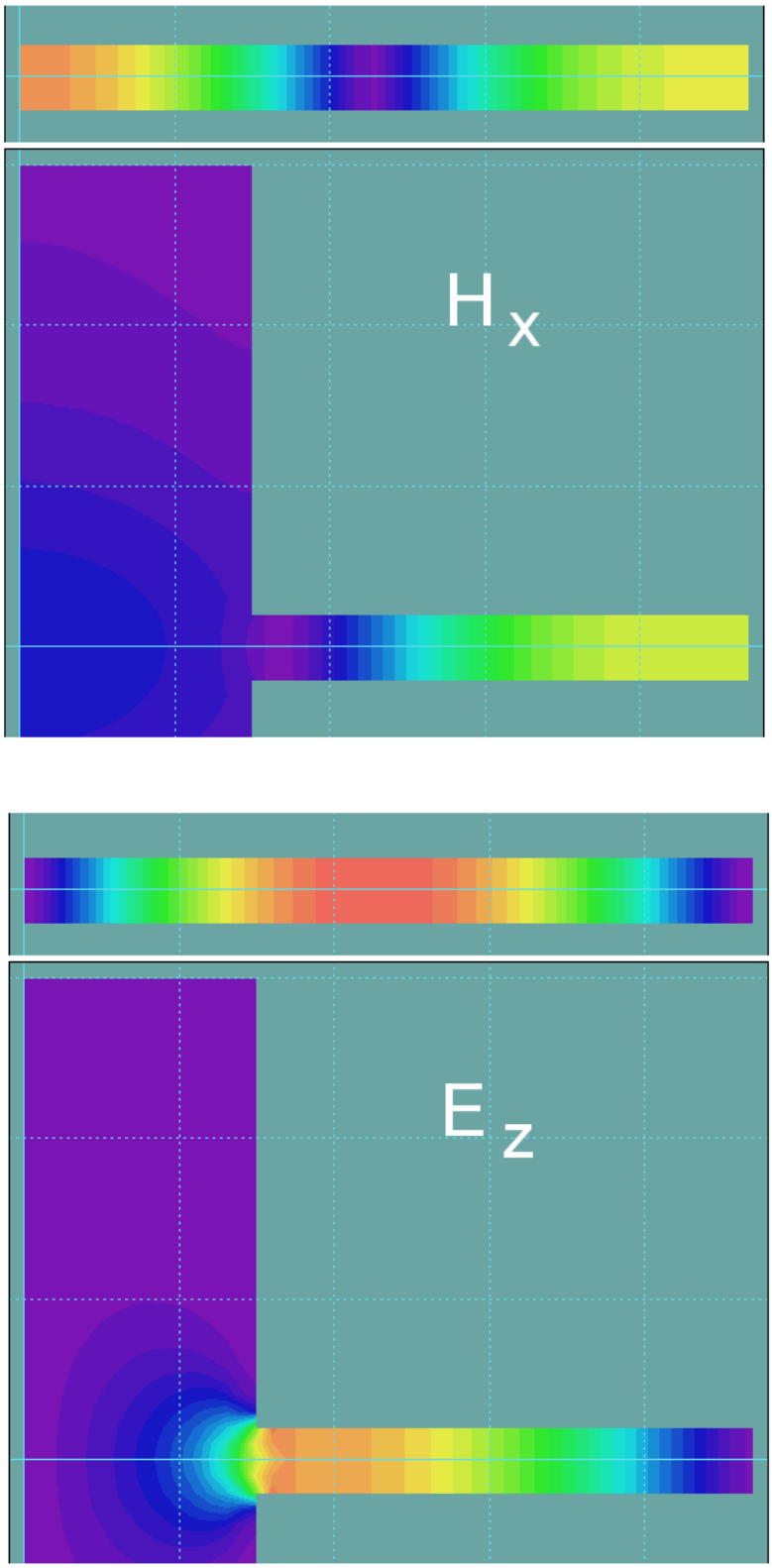

Figure 10: Field variations for the TM110 mode in the plane x = 0.0 cm without and with a beam pipe of radius 7.5 cm (R = 23.5 cm, D = 2.0 cm). Top: $|H_x|$. Bottom: $|E_z|$.

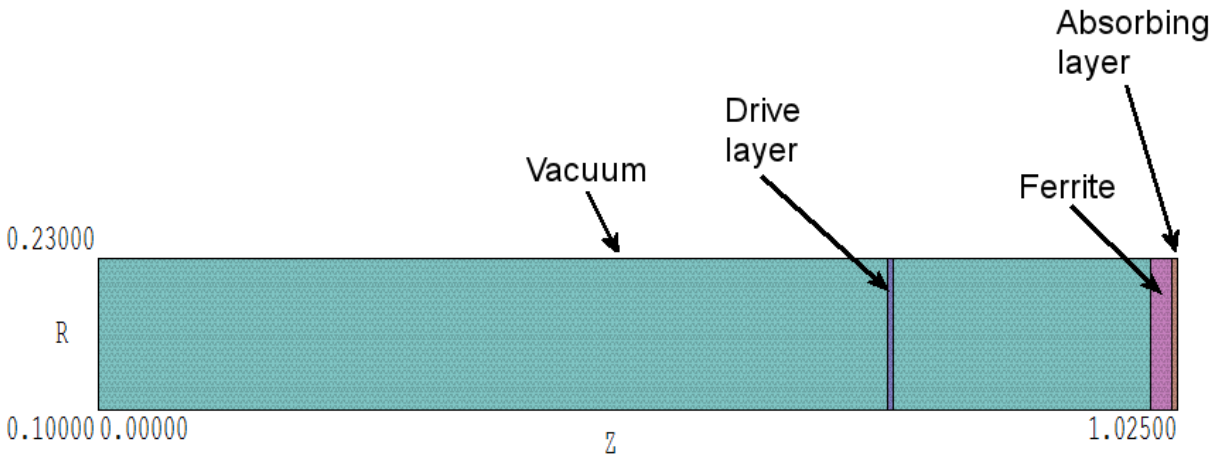

Figure 11: Geometry of the coaxial line test solution.

4 Modeling ferrite boundaries

The model of the ferrite boundary shown in Fig. 1 is critical. The main purpose of this work is to determine how changes in the configuration of ferrites affect the BBU mode. This section reviews the physics of ferrite boundaries and techniques to represent them in a finite-element solution. To begin, I studied the simplest geometry and mode structure, a coaxial transmission line resonator. Here, I could employ the two-dimensional **WaveSim** code. It runs quickly and determines an exact matrix-inversion solution rather than the approximate time-domain method of **Aether**. Figure 11 shows the test geometry, a coaxial line with inner radius $r_i = 0.10$ m and outer radius $r_o = 0.23$ m. The element size for the mesh was 0.005 m. The vacuum section of the line was 1.0 m long. There was a second material region of length 0.02 m. The properties assigned to this region determined the nature of the mode. The solution volume terminated with a single-element layer to absorb traveling waves in the second medium. Modes were excited by a source region at z = 0.75 m that carried a radial current density of the form

$$j_r = A\,\frac{\exp(j2\pi ft)}{r}. \tag{3}$$

Transmission and reflection of waves at the ferrite are determined by its impedance:

$$Z = \sqrt{\frac{\mu_r}{\epsilon_r}}\,Z_o, \tag{4}$$

where μ_r is the relative magnetic permeability of the medium, ϵ_r is the relative dielectric constant and Z_o is the impedance of vacuum, $Z_o = 377.3\ \Omega$. The reflection and transmissions coefficients for the electric field E_r and magnetic field H_θ of a wave incident on the ferrite are given by:

$$R_E = \frac{Z/Z_o - 1}{Z/Z_o + 1}, \quad T_E = \frac{2(Z/Z_o)}{Z/Z_o + 1},$$
$$R_H = \frac{1 - Z/Z_o}{Z/Z_o + 1}, \quad T_H = \frac{2}{Z/Z_o + 1}. \tag{5}$$

where $Z/Z_o = \sqrt{\mu_r/\epsilon_r}$. The wave-reflection properties of the medium are therefore determined by the ratio of μ_r to ϵ_r rather than their absolute values. For a practical electromagnetic calculation, we want to avoid large differences in the speed of light between regions. The speed of light in the ferrite is given by

$$v = \frac{c}{\sqrt{\mu_r\ \epsilon_r}}. \tag{6}$$

In an real ferrite, the large values of μ_r and ϵ_r give a low value of v. The resulting short wavelengths compared to vacuum would require small elements to resolve. We can apply the additional condition:

$$\mu_r\ \epsilon_r = 1 \tag{7}$$

without affecting wave reflection properties. The uniform speed of light throughout the solution volume means that we can use uniform element size. The assumption reduces concerns about Courant stability in the time-domain calculation with **Aether** discussed in following sections.

We can simulate a metal downsteam boundary by setting the ferrite properties to $\epsilon_r = 10^8$ and $\mu_r = 10^{-8}$. In this case, the condition $E_r = 0.0$ holds at both boundaries. The coaxial line becomes a half-wave resonant with $\lambda = 2.0$ m. The theoretical resonant frequency is

$$f = \frac{c}{\lambda} = 149.896 \quad \text{MHz}. \tag{8}$$

A **WaveSim** solution gives $f = 149.896$ MHz. At the opposite extreme, we can set the ferrite to infinite impedance ($\epsilon_r = 10^{-8}$ and $\mu_r = 10^8$.). In this case, the electric field has a maximum at the boundary and $H_\theta = 0.0$. In this case, the system is a quarter-wave resonator with $\lambda = 4.0$ m and $f = 74.948$ MHz. Again, a **WaveSim** yields the expected result.

Next, consider the behavior of an actual ferrite boundary. One challenge is that the property specifications of the DARHT ferrites have been lost to time. Until measurements are available, I will use some reasonable estimates. I purchased TDK PE-14 induction linac cores about 30 years ago. They had a quoted small-signal relative magnetic permeability of $\mu_r = 600$. An internet search of the properties of nickle-zinc ferrites yields values up to $\mu_r = 10000$. Relative dielectric constants are in the range $\epsilon_r = 20$ to 60[3]. The volume resistivity may vary by several orders of magnitude. The ferrites I purchased had $\rho \cong 10^4$ Ω-m. At a frequency of 800 MHz, the skin depth is approximately 7.0 cm.

[3]G. Ranga Mohan, D. Ravinder, A.V. Ramana Reddy and B.S. Boyanov, *Dielectric properties of polycrystalline mixed nickel-zinc ferrites*, Materials Letters **40** (1999), 39.

For a physical model, I assume that the standing wave in the resonator consists of the superposition of two traveling waves of half amplitude. When the forward-going wave strikes the ferrite boundary, a portion of the energy continues as a traveling wave according to transmission coefficients of Eq. 5. Another assumption is that in the DARHT cavity, energy transmitted to the long ferrite stack does not return to contribute to the BBU mode. There are three reasons:

- Wave energy is absorbed because of the material volume resistivity and complex components of μ and ϵ.
- Because of the low speed of light in the ferrite, the electromagnetic transit time is much longer than the period of the transverse mode.
- There is a wide range of possible propagation paths.

In the numerical models, I represented the ferrite as a high impedance medium with values of μ_r and ϵ_r adjusted so that $v = c$. For example, with physical values $\mu_r = 1200$ and $\epsilon_r = 20$, the material impedance is $Z = \sqrt{60}/Z_o = 7.746 Z_o$. The adjusted values for use in the code are:

$$\mu_r = \sqrt{60} = 7.746, \quad \epsilon_r = 1/\sqrt{60} = 0.1291. \tag{9}$$

To fulfill the condition that waves do not return, I terminated the ferrite with an ideal absorbing layer. As described in Sect. 13.1 of my book **Field Solutions on Computers**, the absorbing layer has μ_r and ϵ_r matched to those of the ferrite and an electrical conductivity given by

$$\sigma = \frac{1}{Z\Delta} = \frac{1.0}{(7.746)(377.3)(0.005)} = 0.0684 \ \ \text{S/m}, \tag{10}$$

where Δ is the thickness of the layer.

The **WaveSim** calculation confirmed the features of the model. The first run was set to make a frequency scan from 50.0 to 100.0 MHz in one-hundred steps. Figure fig:coaxfreq shows the probe signal compared to that for the open-circuit boundary (a quarter-wave resonator). As expected, the resonance frequency with the high-impedance ferrite (75.312 MHz) was close to the infinite-impedance result (74.948 MHz). The width of the response curve contributed by the ferrite was a 11.9 MHz. The corresponding quality factor is Q = 75.312/11.9 = 6.33. The quality factor can also be calculated from total integrals of field energy and power loss. A **WaveSim** run in the resonance mode gaves a total field energy in the vacuum regions if $U = 2.11 \times 10^{-9}$ J and total power dissipated in absorption layer of $P = 0.1639$ W. The value imply a quality factor

$$Q = \frac{2\pi f U}{P} = \frac{2\pi(75.31 \times 10^6)(2.11 \times 10^{-9})}{0.1639} = 6.09. \tag{11}$$

I made an additional calculation with an elongated ferrite region. The length had no effect on the resonant frequency and vacuum region solution. An axial field scan of $|E|$ confirmed that there was a standing wave in the vacuum region (*i.e.*, varying amplitude)

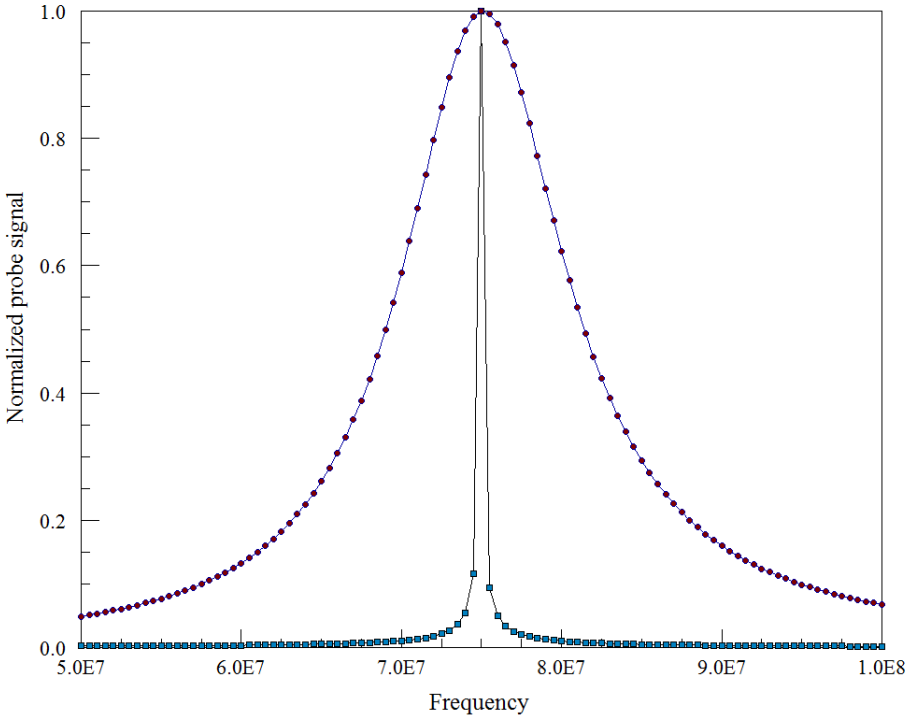

Figure 12: Probe response as a function of frequency for the coaxial resonator. Blue: open-circuit termination. Red: ferrite with $Z/Z_o = 7.746$.

and a pure traveling wave in the ferrite (*i.e.*, fixed amplitude). The Q values implied by Fig. 12 and Eq. 11 are consistent with the physical model of transmission of the positive-going resonator wave. The product of the transmission coefficients of Eq. 5 for $Z/Z_o = 7.46$ is $T_E \times T_H = 0.405$. If D is the cavity length and S_o is the magnitude of the Poynting vector of the positive-going wave, then the total energy lost in one period from the quarter wave resonator is proportional to $4DS_o \times 0.405$. The total energy in the resonator (U) is proportional to $D(2S_o)$. An alternate defintion of the quality factor is $2\pi U/$(Energy lost in one period). By this reasoning, a rough estimate of the quality factor is given by

$$Q \cong \frac{2\pi(2S_oD)}{4(0.405)S_o} = 7.75. \tag{12}$$

5 Cylindrical cavity with a ferrite boundary

This section describes calculations where the ferrite boundary model is applied to a test cylindrical cavity ($R = 23.5$ cm, $D = 3.0$ cm) to get a sense of the Q values expected in the DARHT Mod2 cavities. I made an initial test to make sure that the model gave the correct results in **Aether** by making a comparison calculation with **WaveSim**. For this calculation, I used the circularly-symmetric TM_{010} mode. The element size was 0.25 cm for the **WaveSim** calculation and 0.50 cm for the **Aether** solution. In both cases, the ferrite was represented by a layer two elements thick on the outer boundary surrounded by a one-element-thick absorbing layer. Absorbing layers in **Aether** must be adjacent to an open boundary, so I included void elements on the outside. Figure 13 shows the mesh. For the average thickness of the absorbing layer in the **Aether** calculation, I multiplied the element size by the average of $\cos\theta$ from $\theta = 0^o$ to 45^o. The result was 0.563 cm.

The theoretical resonant frequency for a metal cavity is $f_{010} = 488.30$ MHz. With outer elements set to the metal property, **WaveSim** returned a value of 488.22 MHz and **Aether** 487.40 MHz. I also set up calculations with a open-circuit boundary condition (ideal ferrite). In this case, the radial variation is more complex – there are maxima of the electric field at the axis and wall. The resonant mode should have a frequency between that of the TM_{010} and TM_{020} (1120.8 MHz) modes. I will use the notation $TM_{01.50}$ to refer to the mode. The resonant frequencies from **WaveSim** and **Aether** were 777.86 MHz and 778.40 MHz respectively.

For a high (but finite) ferrite impedance, we expect a resonant frequency near that of the open-boundary solution. With the choice $Z/Z_o = 7.746$, **WaveSim** returned a resonant frequency of 777.63 MHz. The values of volume-integrated field energy and power dissipated in the absorber gave a value $Q = 14.87$. For comparison, the **Aether** calculation gave $f_{01.50} = 773.23$ MHz and a quality factor determined from energy and power integrals of $Q = 16.51$. The agreement is close considering the relatively coarse meshing of the circular absorption region in the three-dimensional solution. Figure 14 shows the field pattern of the **Aether** calculation. I also made calculations with a higher ferrite impedance, $Z/Z_o = 20.0$. In this case, the calculated Q values were 37.5 (**WaveSim**) and 44.73 (**Aether**). The values imply that Q is roughly proportional to the ferrite impedance.

We can also infer Q values from the frequency width of the probe responses. Figure 15 shows the Aether results for the open-circuit cavity and a ferrite boundary with impedances of $Z/Z_o = 7.746$ and 20.0. As in Fig. 3, the full-width at half-maximum for the open-boundary cavity (no damping) had a non-zero value of 18 MHz, setting an accuracy limit for estimates of Q. For a rough approximation, we can subtract this width from that of damped solutions. With this condition, I estimated Q values of 11.6 for $Z/Z_o = 20.0$ and 43 for $Z/Z_o = 7.746$, consistent with results from the solution integrals.

To conclude the section, I will discuss an **Aether** calculation of the BBU mode in a cylindrical cavity with ferrite boundary. With open circuit boundary, we expect to observe a frequency between the metal-cavity modes $f_{110} = 778.6$ MHz and $f_120 = 1425.5$ MHz. I used the half-cavity model discussed in Sect. 2. The resonant frequency with $Z/Z_o = 7.746$ was 1078.3 MHz. Figure 16 shows the resulting field pattern in the plane $z = 0.0$. At the high-impedance boundary, the quantity **H** was close to zero **E** had a non-zero value. The net effect is to compress the field pattern toward the axis compared to the metal-walled cavity;

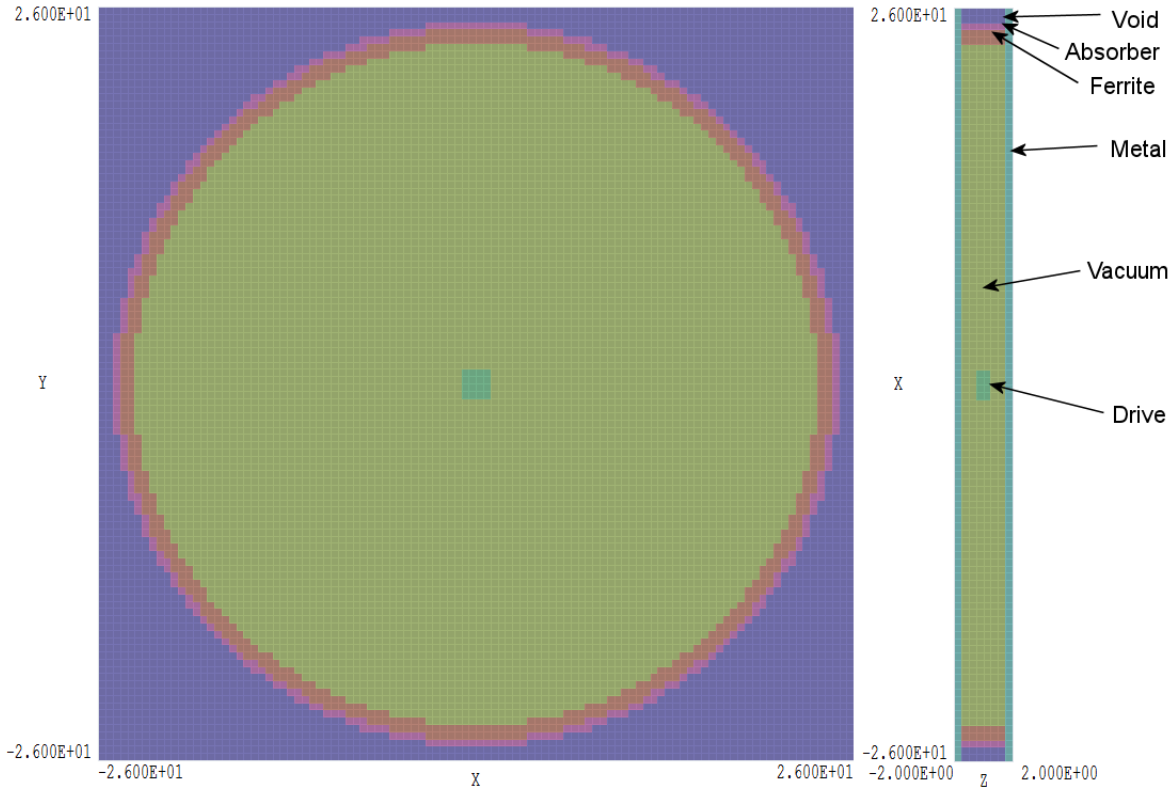

Figure 13: **Aether** mesh for the TM_{010} mode in a cylindrical cavity with a ferrite boundary.

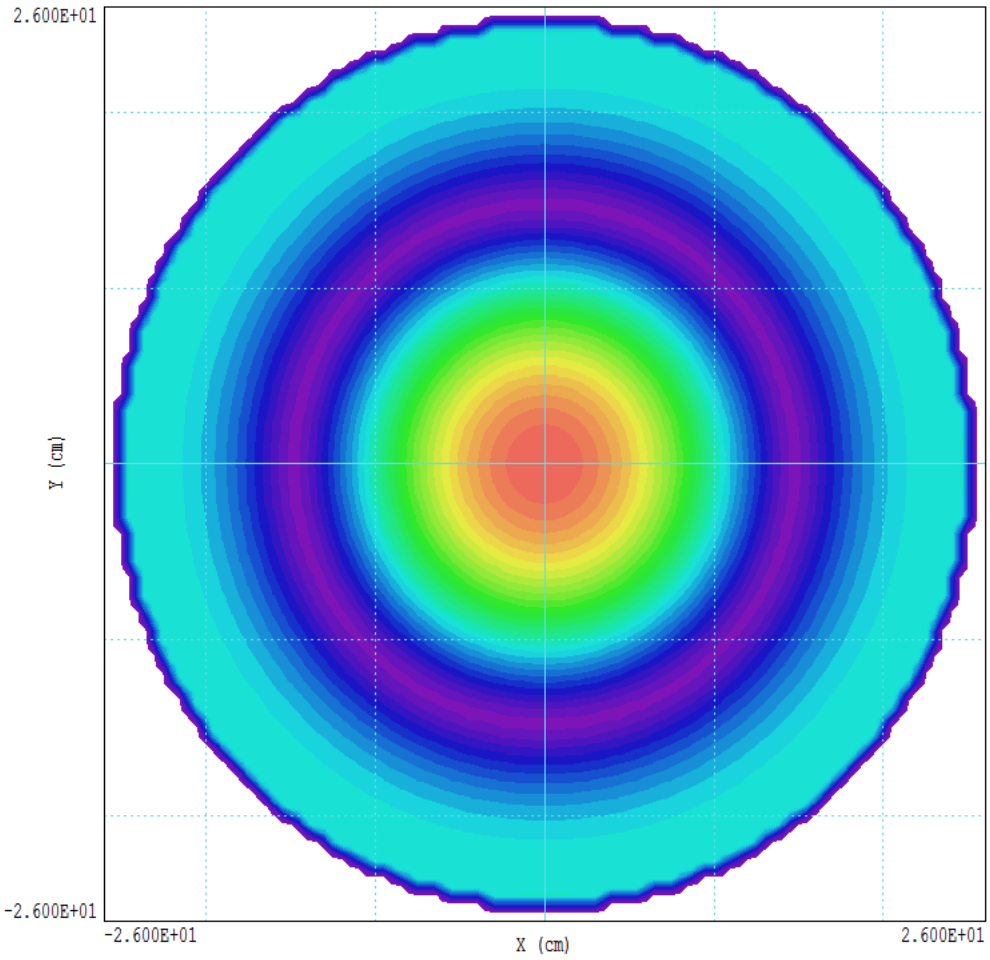

Figure 14: **Aether** calculation of $|E_z|$ for the $TM_{01.50}$ mode in a cylindrical cavity. Plot in the plane $z = 0.0$ cm.

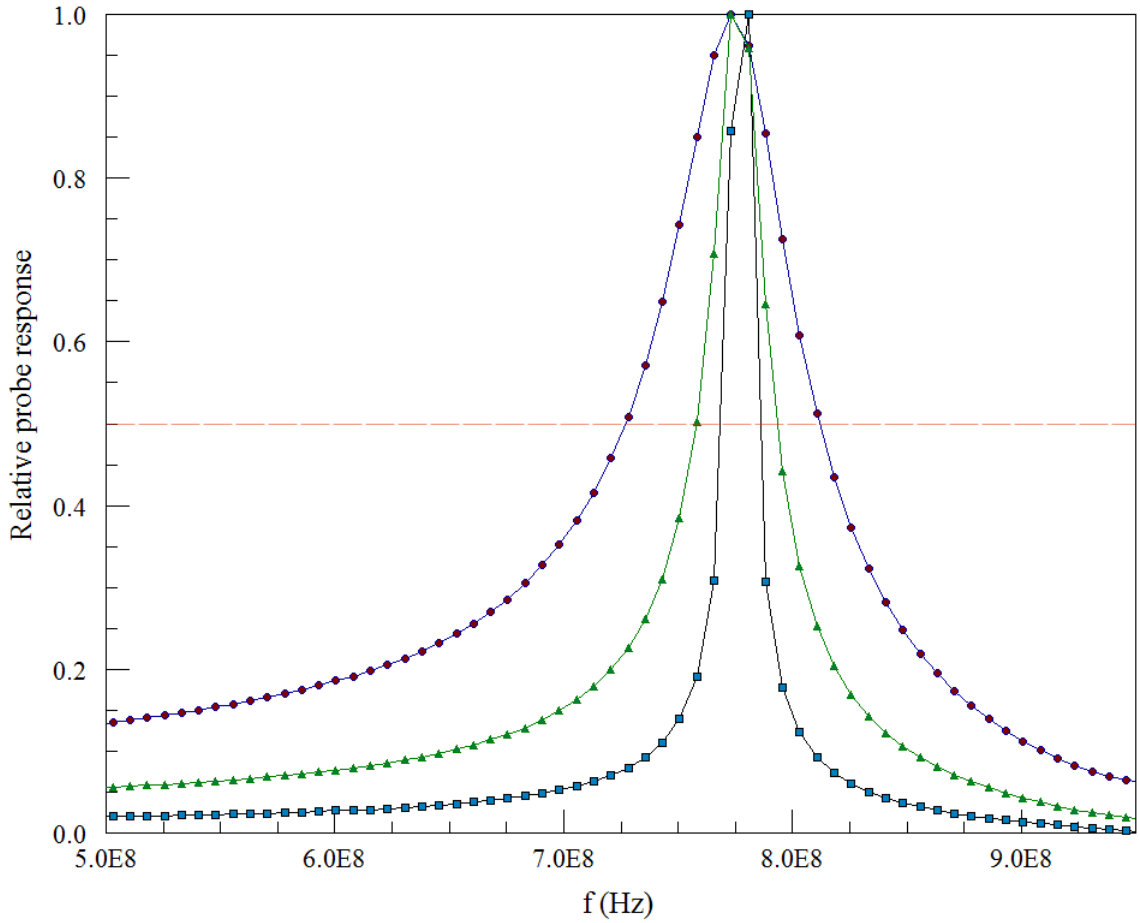

Figure 15: Probe response for **Aether** resonant mode calculations of the $TM_{01.50}$ mode. Blue: open circuit, Green: ferrite impedance $Z/Z_o = 20.0$. Red: ferrite impedance $Z/Z_o = 7.746$.

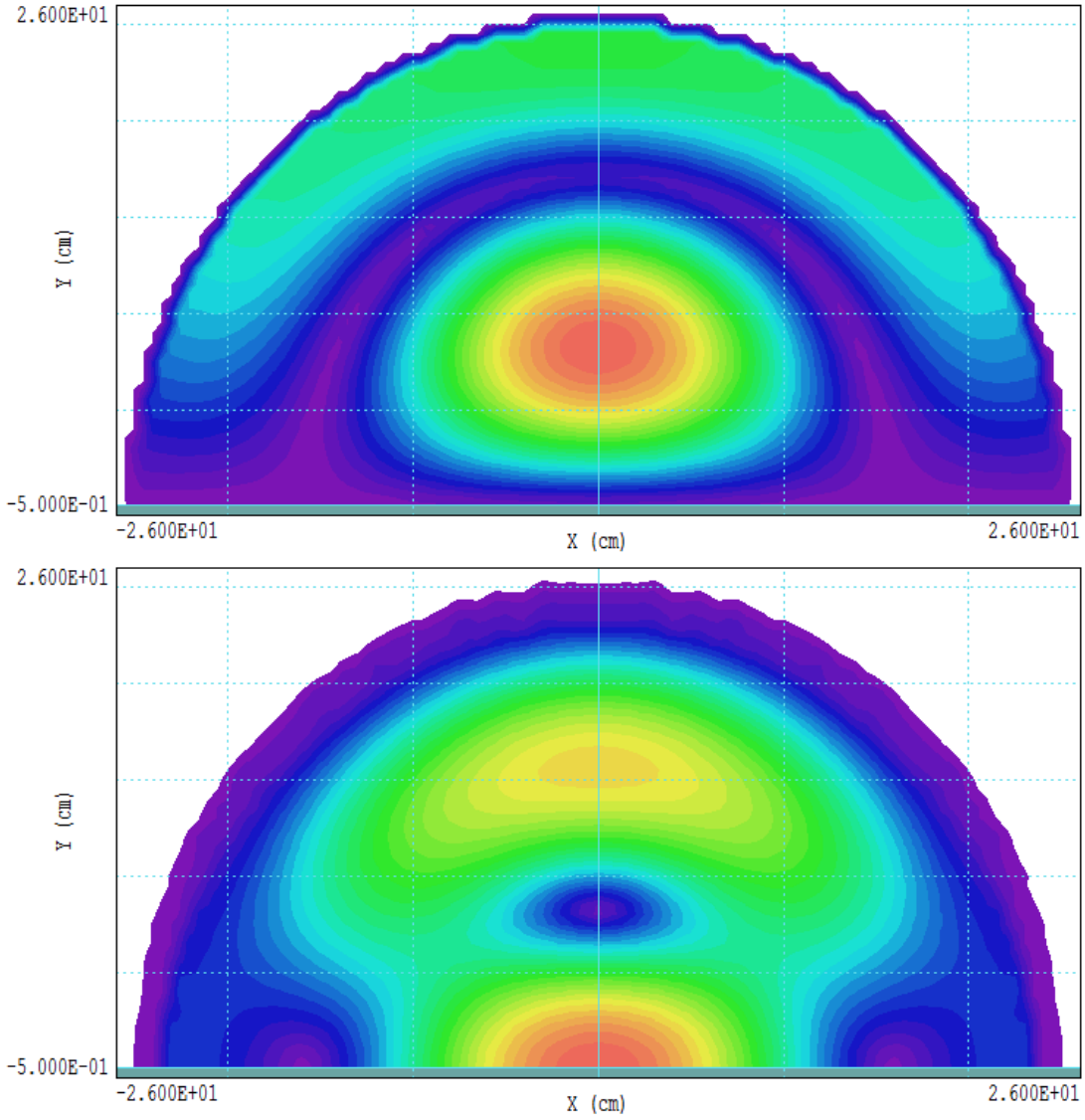

Figure 16: TM1150 mode in a cylindrical cavity with a high-impedance boundary. Plots in the plane z = 0.0 cm. Top: —E—. Bottom: —H—.

hence, the higher frequency. The Q value estimated from energy/power volume integrals was $Q = 19.8$. With a ferrite impedance of $Z/Z_o = 20.0$, the Q value increased to 52.7. Again, Q was approximately proportional to Z/Z_o.

6 DARHT Mod2 cavity model

After the lengthly preamble, creating a model of the DARHT Mod2 cavity was straightforward. Figure 18 shows the mesh for the **Aether** calculation. As in Sect. 3, I used a half-plane representation with a metal boundary at $y = 0.0$ cm and extended beam pipe apertures terminated with a metal boundaries. The excitation source was located near the expected point of maximum electric field and carried a current density component j_y. I included a second source at large radius to experiment with a dual drive with a 180° phase difference. It was not used for the calculations of this report. Most of the parts were turnings, with boundaries described by a set of short vectors that I determined from a cavity drawing supplied by LANL. The outer region included the exposed ferrite (a layer three elements thick), an single-element absorbing layer and a void region to set a boundary condition behind the absorber. In the **Aether** calculation, the insulator had a relative dielectric constant of $\epsilon_r = 2.53$ and the transformer oil had $\epsilon_r = 2.2$. I found solutions for two values of ferrite impedance, $Z/Z_o = 7.746$ and 20.0. Each solution involved a resonance search and then a field calculation at the determined frequency. Solution times were longer than the test examples of previous sections because of the larger solution volume and smaller element size: 1140 s for the resonant solution and 228 s for the field solution.

Figure 17 shows the probe response in the resonant calculation for $Z/Z_o = 7.746$ and Figure 19 shows corresponding field distribution in the plane $x = 0.0$ cm . The clean probe response and the resemblance to the field distribution of Fig. 10 gives confidence that solution corresponds to the $TM_{11.50}$ mode. The effects of the beam pipe and the high-impedance boundary are consistent with the discussions of Sects. 3 and 5.

Table 1: Solutions for the $TM_{11.50}$ mode in the DARHT Mod2 cavity.

Z/Z_o	f1150	Q
7.746	704.8 MHz	42.1
20.000	700.0 MHz	106.7

An interesting result is that the Q values listed in Table 1 are significantly higher than those for a cylindrical cavity with a ferrite boundary. This is not the result of differences in the relative absorption area of the ferrite. I verfied that the ratio of ferrite area to cavity volume for the two configurations was about the same: .085 cm^{-1} for the cylindrical cavity and 0.100 cm^{-1} for DARHT cavity. Rather, the difference is the result of the mode field morphology. Figure 20 plots the spatial distribution of electromagnetic field-energy density in the plane $x = 0.0$ for two configurations. The red lines indicate the surface of the ferrite. In the case of the DARHT cavity, the ferrite surface is in a backwater with respect to the

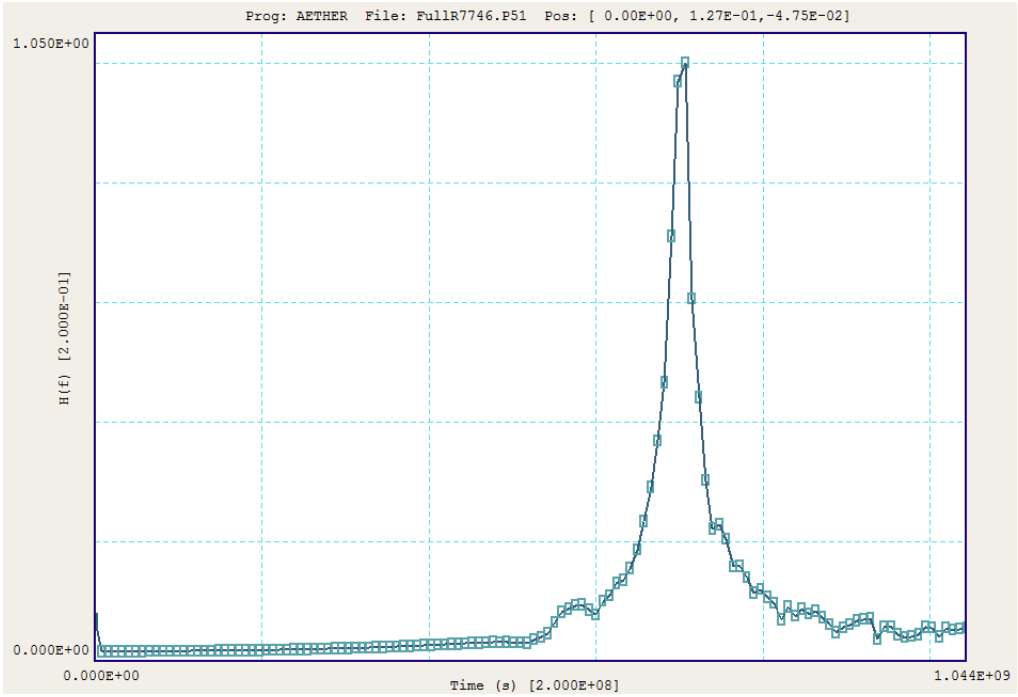

Figure 17: Probe response for the DARHT Mod2 cavity with $Z/Z_o = 7.746$.

mode fields, so the energy flux is low. A favorable implication is that adjustments to the cavity geometry near the ferrite may have a significant effect on the mode Q.

7 DARHT Mod2A comparison

Figure 21 shows the geometry of the Mod2A DARHT cavity. The main difference from the Mod2 geometry is the re-entrant area near the face of the ferrite stack (arrow at the right). There is also the option to include a ferrite damping ring with a wedge shaped cross section near the vacuum insulator (arrow on the left). The following section discusses the effect of the damping ring on the BBU mode.

The resulting field patterns were quite similar to those of the Mod2 cavity. Figure 22 shows the computational mesh and the distribution of field energy for the $TM_{01.50}$ mode. Again, the energy density is low near the ferrite surface. Table 2 shows a comparison of the mode characteristics for the two geometries with ferrite impedances of $Z/Z_0 = 7.746$ and $Z/Z_0 = 20.0$. (Note that the absolute values of field energy and dissipated power are not significant in a resonant type **Aether** solution.) There was a small difference in frequency, about 0.5%. The Q values in the Mod2A cavity were higher because the ferrite face was farther from the main cavity volume.

Finally, Fig. 23 shows a plot of $B_x(0.0, 0.0, z)$ of the $TM_{01.50}$ mode for the two cavity geometries with ferrite impedances of $Z/Z_0 = 7.746$ and 20.0. For the comparison, the electromagnetic field energy was normalized to 1.0 J. There was a small difference between the geometries because of difference in the field distributions. The ferrite impedance had no discernable effect.

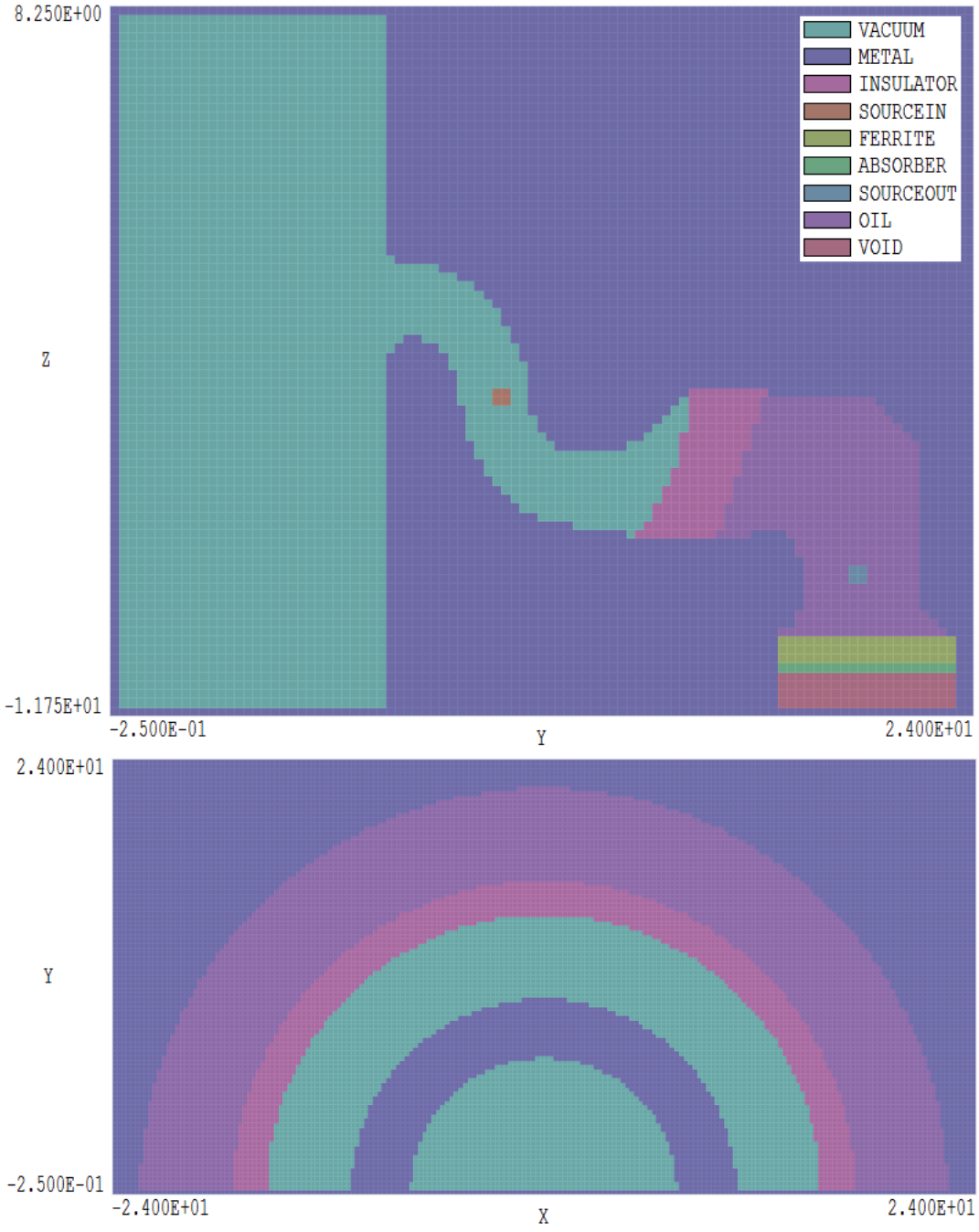

Figure 18: **MetaMesh** plots of the DARHT Mod2 cavity mesh. Dimensions in cm, cubic elements with length 0.25 cm. Top: View in the plane $x = 0.0$ cm. Bottom: view in the plane $z = -5.5$ cm.

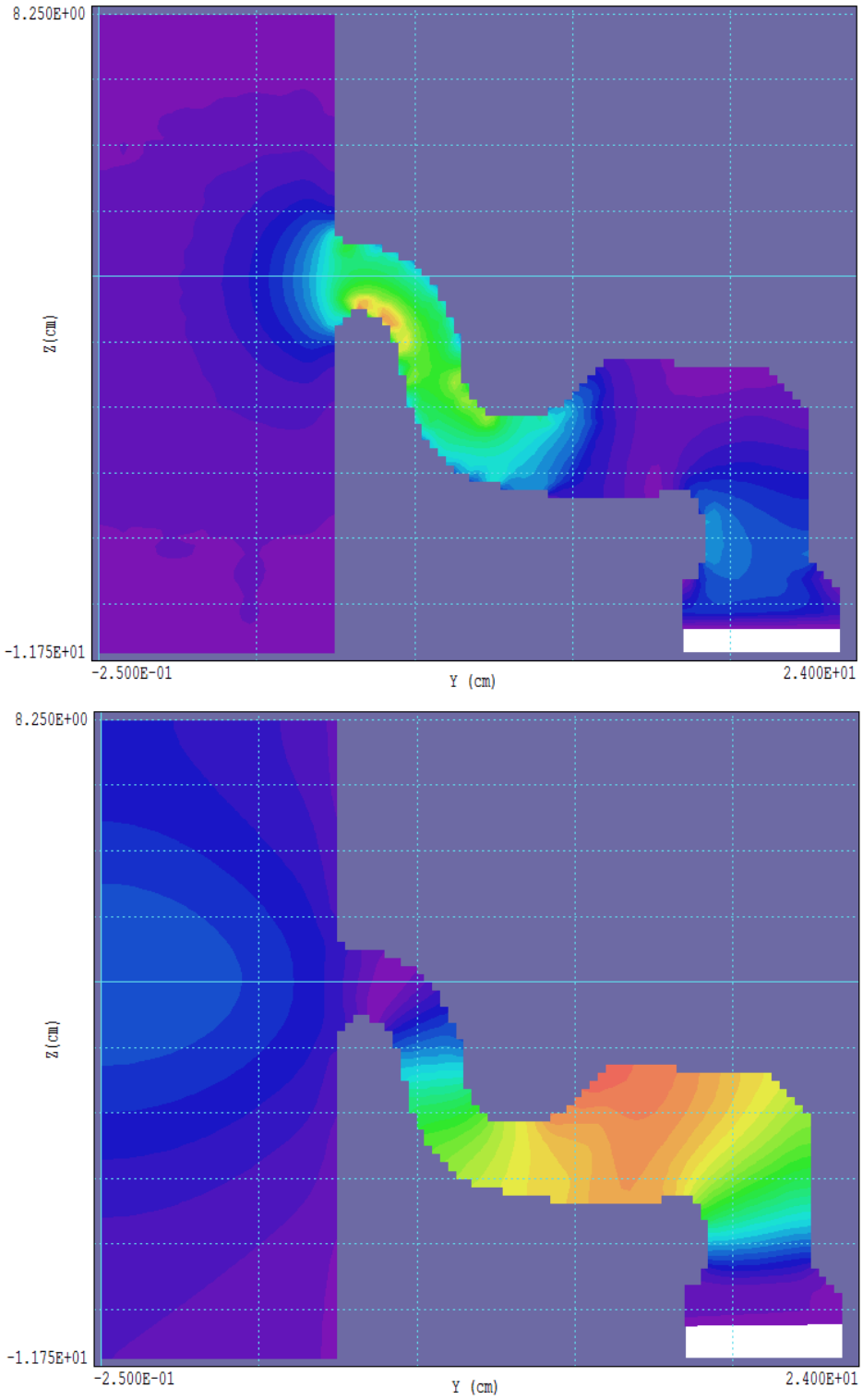

Figure 19: Field distribution for the $TM_{01.50}$ mode in the DARHT Mod2 cavity. Top: $|\mathbf{E}|$. Bottom: $|\mathbf{H}|$.

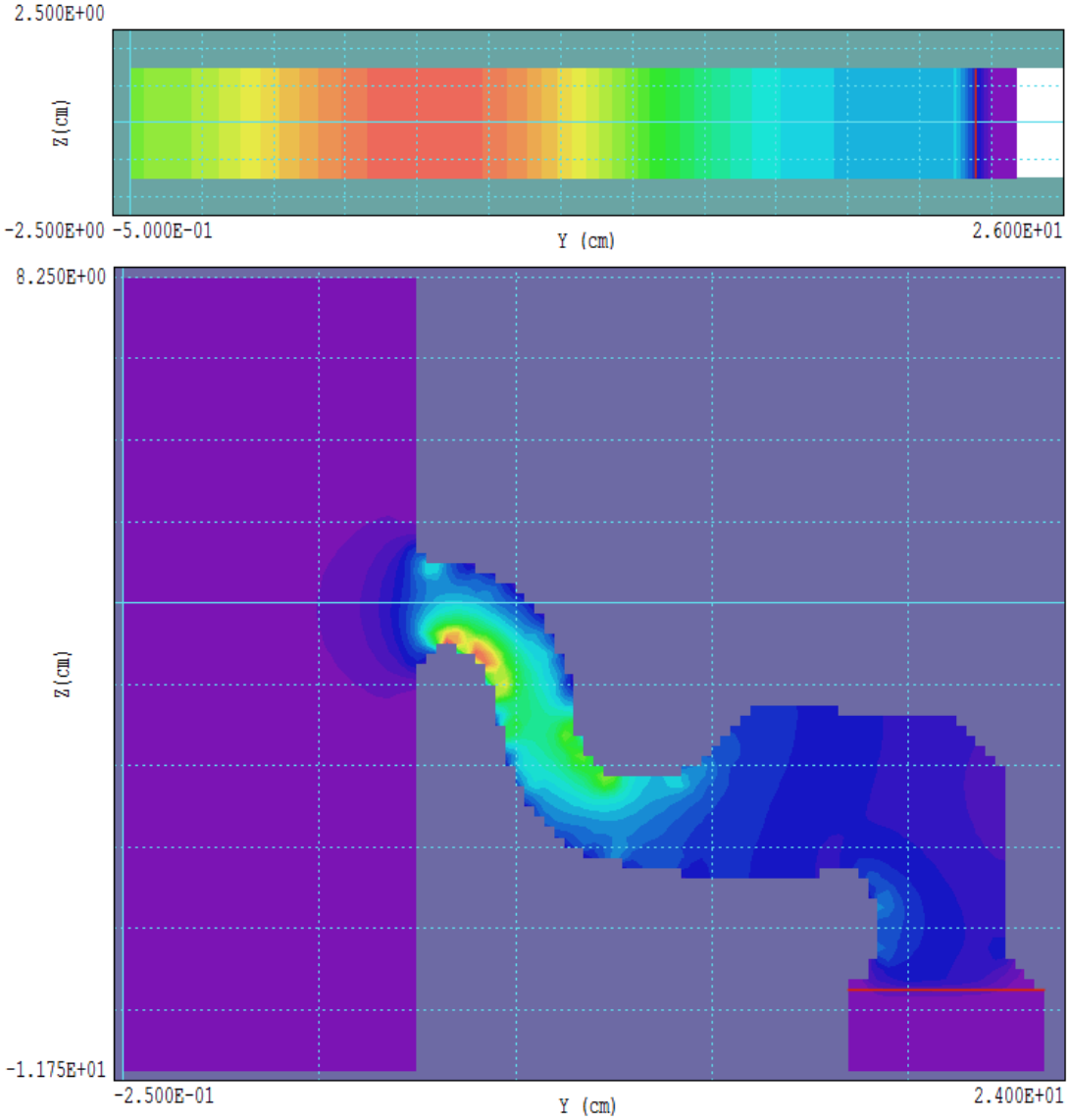

Figure 20: Field energy density distributions, plots in the plane $X = 0.0$ cm. Top: cylindrical cavity. Bottom: DARHT Mod2 cavity,

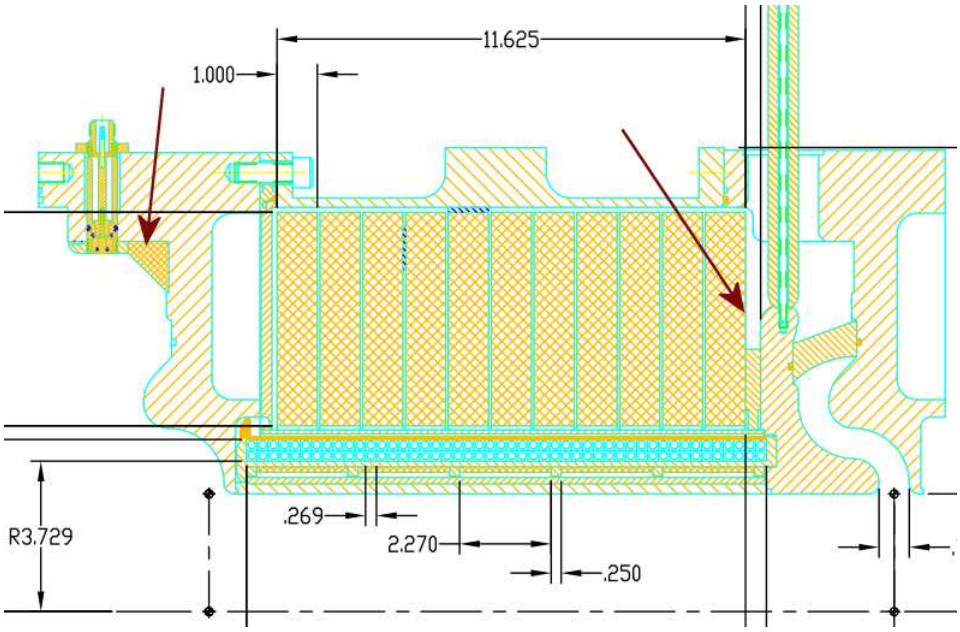

Figure 21: Mod2A cavity geometry. The arrow on the right indicates the re-entrant region at the ferrite-stack face. The arrow on the left shows a ferrite damping ring.

Table 2: Comparison of $TM_{01.50}$ mode characteristics in the Mod2 and Mod2A geometries.

Mod2 cavity				
Impedance Z/Z_0	Field energy (J)	Power (W)	Frequency (MHz)	Q
7.746	1.53129×10^{-16}	1.61481×10^{-08}	704.75	41.99
20.00	3.88389×10^{-16}	1.60383×10^{-08}	699.92	106.50
Mod2A cavity				
Impedance Z/Z_0	Field energy (J)	Power (W)	Frequency (MHz)	Q
7.746	1.77437×10^{-16}	1.58633×10^{-08}	707.55	49.73
20.00	3.80850×10^{-16}	1.34234×10^{-08}	708.94	126.41

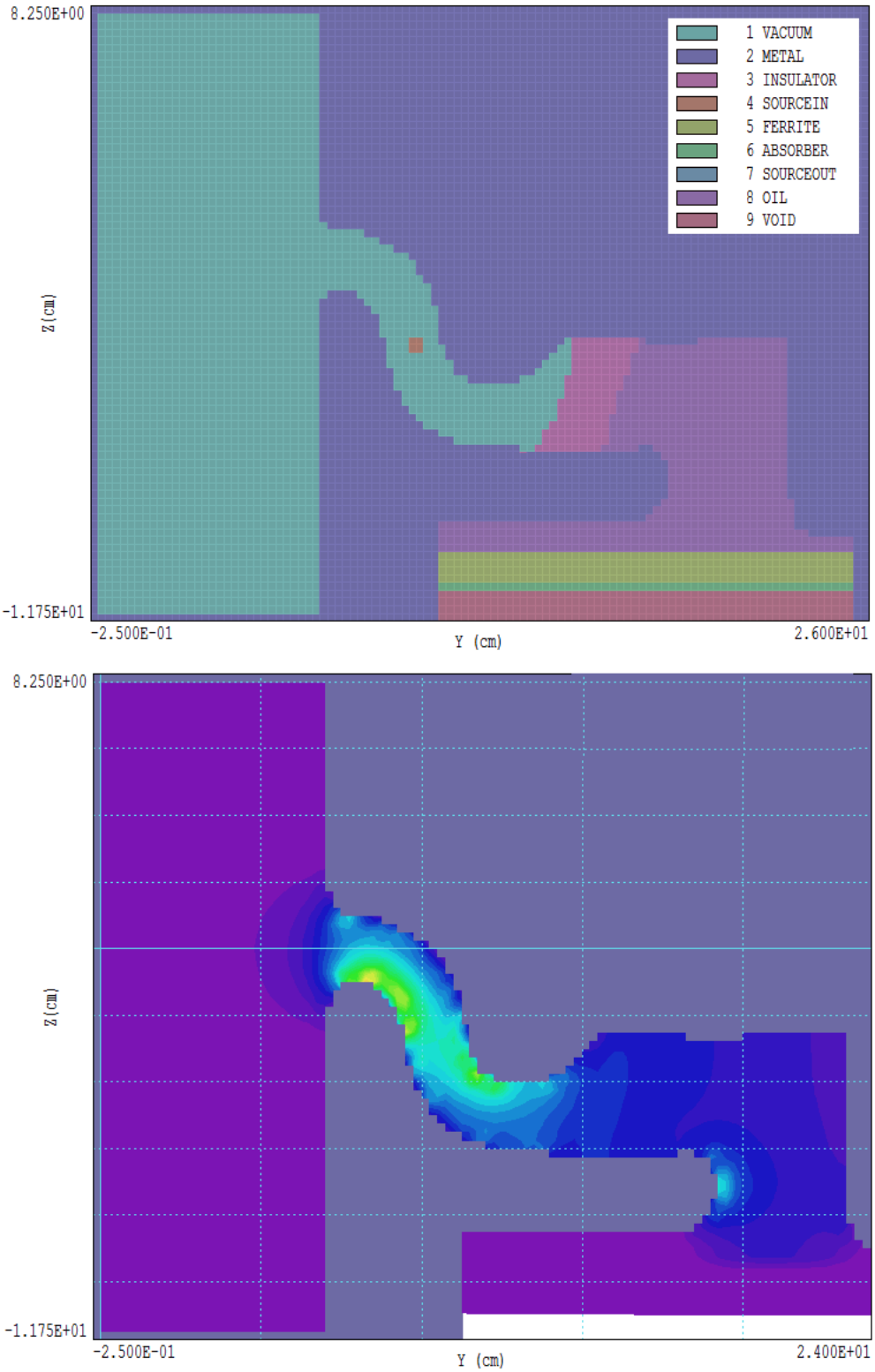

Figure 22: Mod2A cavity modeling, projections in the plane $x = 0.0$ cm. Top: computational mesh. Bottom: distribution of field energy density, u.

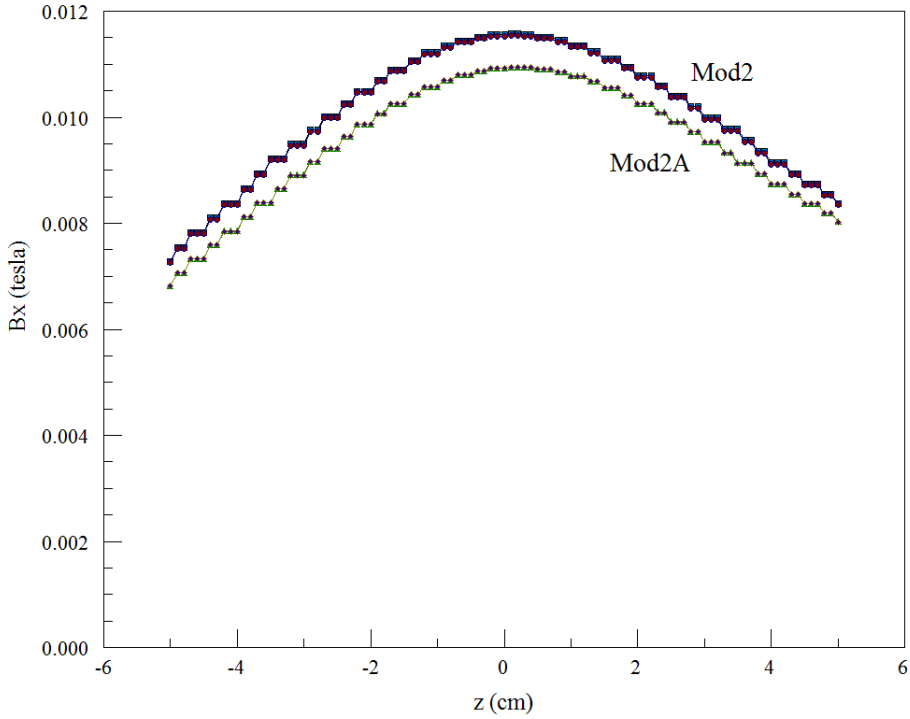

Figure 23: Scan of the deflecting magnetic field B_x along the z axis for the two cavity geometries with a normalized electromagnetic field energy density of 1.0 J. Calculations were performed for $Z/Z_0 = 7.746$ and 20.0.

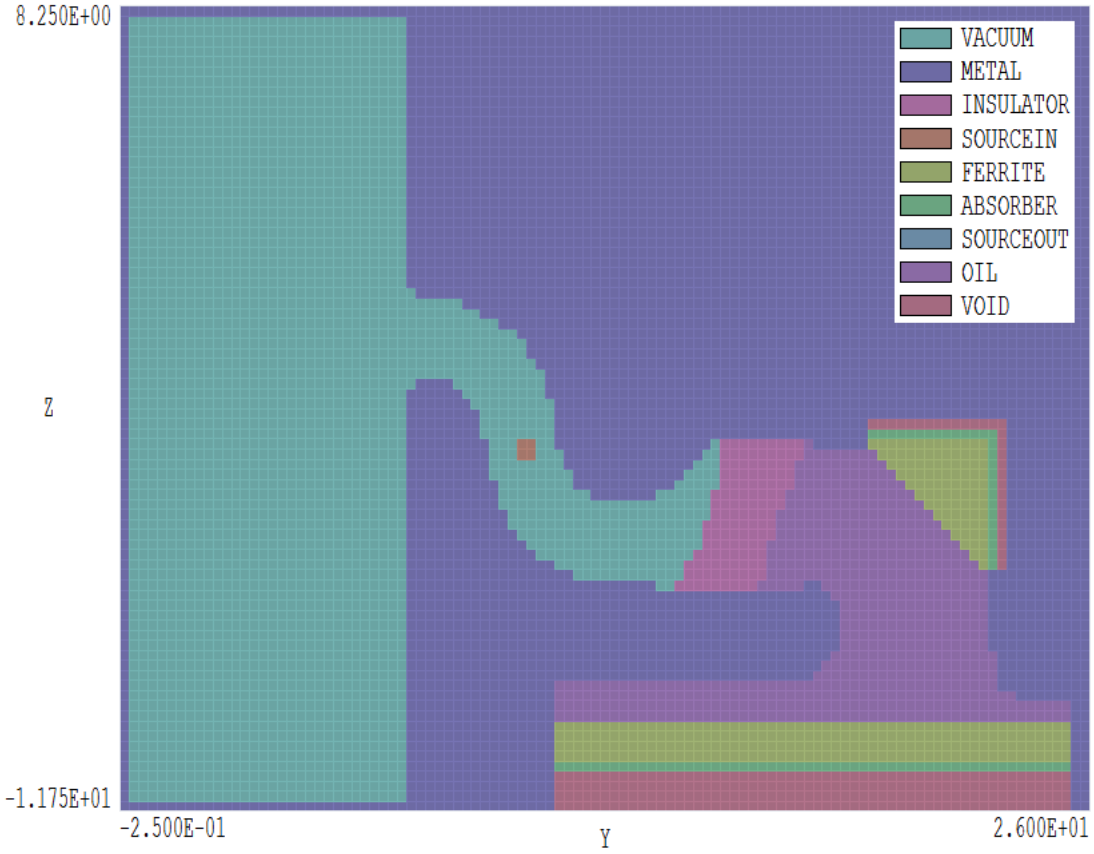

Figure 24: Mesh for the Mod2A cavity with ferrite ring.

8 Mod2A cavity with damping ring

To conclude the series, I added the ferrite wedge to the Mod2A geometry (Fig. 21). As in previous calculations, I assumed that 1) the ferrite had a relative impedance $Z/Z_0 = 7.746$, 2) the electromagnetic propagation velocity was c and 3) all transmitted wave energy was absorbed. Figure 24 shows the computational mesh. An absorbing layer and void region were added at the ferrite-ring boundary to minimize reflected energy. The ring had a strong effect, raising the resonant frequency from 707.55 MHz to 836.01 MHz. Figure 25, plots of the distribution of $|\mathbf{H}|$ without and with the ring, shows the reason. The ring acts as an inductive choke on wall current so that the mode energy was confined to a smaller volume. Also, note how the magnetic field extends farther into the drift tube at the higher frequency. The ring shields the main ferrite stack from the mode fields. Therefore, the Q value with the ring is actually higher, 54.43 compared to 49.73.

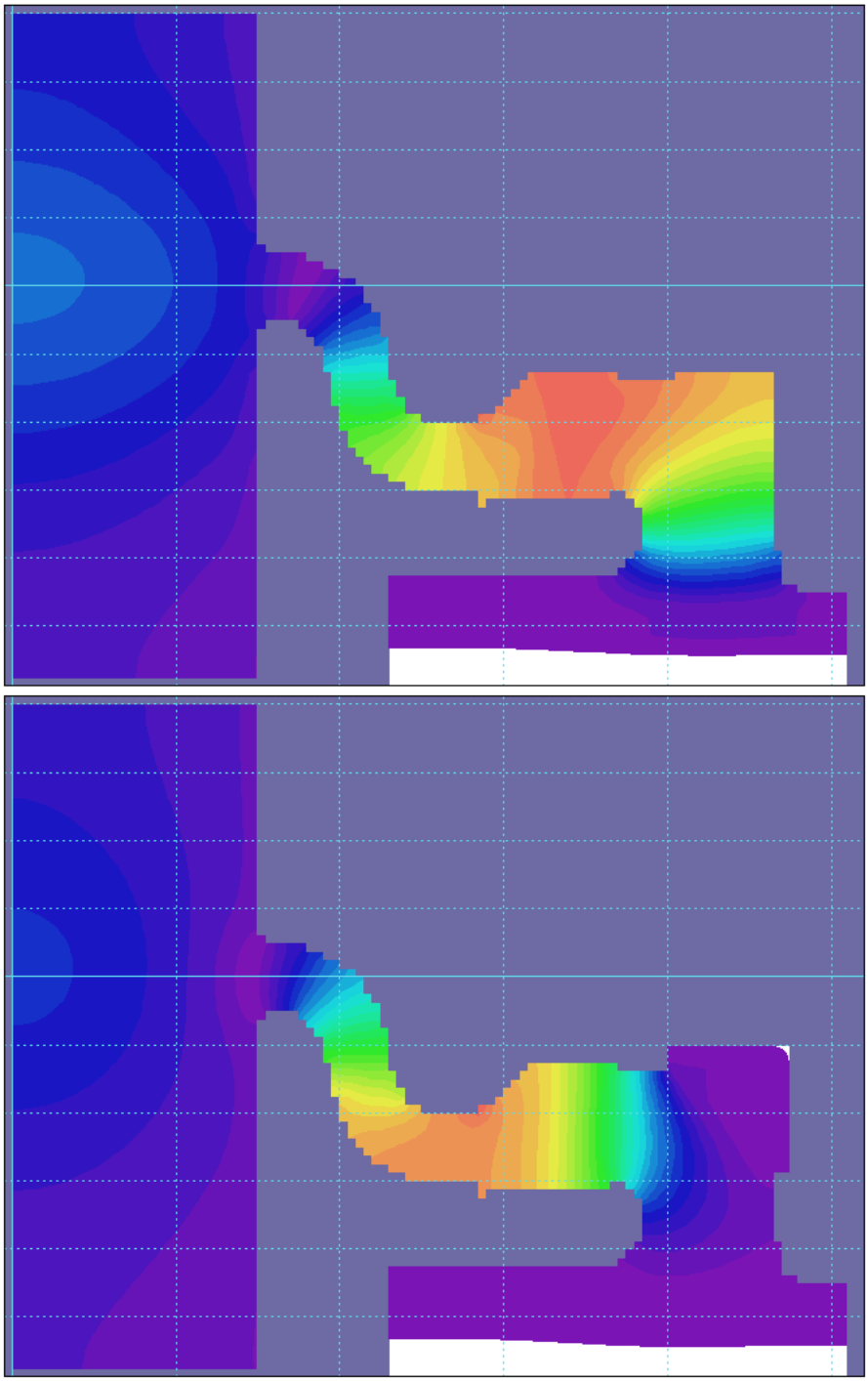

Figure 25: Distribution of $|\mathbf{H}|$ for the $TM_{01.50}$ mode in the Mod2A cavity without (top) and with (bottom) the ferrite ring.